

Provided for non-commercial research and education use.  
Not for reproduction, distribution or commercial use.



This article appeared in a journal published by Elsevier. The attached copy is furnished to the author for internal non-commercial research and education use, including for instruction at the authors institution and sharing with colleagues.

Other uses, including reproduction and distribution, or selling or licensing copies, or posting to personal, institutional or third party websites are prohibited.

In most cases authors are permitted to post their version of the article (e.g. in Word or Tex form) to their personal website or institutional repository. Authors requiring further information regarding Elsevier's archiving and manuscript policies are encouraged to visit:

<http://www.elsevier.com/copyright>



Contents lists available at ScienceDirect

## Journal of Sound and Vibration

journal homepage: [www.elsevier.com/locate/jsvi](http://www.elsevier.com/locate/jsvi)

# A general procedure for the dynamic analysis of finite and infinite beams on piece-wise homogeneous foundation under moving loads

Zuzana Dimitrovová\*

UNIC, Department of Civil Engineering, Faculdade de Ciências e Tecnologia, New University of Lisbon, Monte de Caparica, 2829-516 Caparica, Portugal

## ARTICLE INFO

*Article history:*

Received 24 April 2009

Received in revised form

12 January 2010

Accepted 13 January 2010

Handling Editor: H. Ouyang

Available online 6 February 2010

## ABSTRACT

Transversal vibrations induced by a load moving at a constant speed along a finite or an infinite beam resting on a piece-wise homogeneous visco-elastic foundation are studied. Special attention is paid to the amplification of the vibrations which arise as the point load traverses a foundation discontinuity. The governing equations of the problem are solved by the normal-mode analysis. The solution is expressed in the form of an infinite sum of orthogonal natural modes multiplied by the generalized displacements. The natural frequencies are obtained numerically exploiting the concept of the global dynamic stiffness matrix. This ensures that the frequencies obtained are accurate. The methodology is neither restricted by load velocity nor damping and is simple to use, though obtaining the numerical expression of the results is not straightforward. A general procedure for numerical implementation is presented and verified. There is no restriction for finite structures, however, for infinite structures, validity of the results is restricted to a “region of interest” of finite length. To illustrate the methodology, the probability of exceeding an admissible upward displacement is determined when the load travels at a certain velocity according to the normal distribution. In this problem, the given structure has an intermediate part of adaptable foundation stiffness, which is optimized in a parametric way, enabling to draw important conclusions about the optimum intermediate stiffness. The results obtained have direct application on the analysis of railway track vibrations induced by high-speed trains crossing regions with significantly different foundation stiffness.

© 2010 Elsevier Ltd. All rights reserved.

## 1. Introduction

The rapid growth of high-speed railway networks and the considerable evolution of train vehicles capable to operate at more than  $500 \text{ km h}^{-1}$  created a number of related problems that have motivated a significant amount of scientific work. The amplification of train-induced vibrations, caused by inhomogeneities in the track foundation, is one of these issues still demanding further attention. The theoretical basis of this phenomenon lies in the fact that, when the load passes with a constant velocity over a discontinuity in the supporting structure, additional vibrations, conventionally referred to as transition radiations, are generated. These vibrations can significantly amplify the deflection field in the beam and aggravate track deterioration; hence, concerns related to the vehicle stability and passengers comfort should be taken into account.

\* Tel.: +351 212948580x10341; fax: +351 212948398.

E-mail address: [zdim@fct.unl.pt](mailto:zdim@fct.unl.pt)

Non-homogeneous foundation stiffness can be originated by geotechnical conditions, by track degradation or by alterations of the structural design. Such changes can be quite sharp and, in consequence, the track settlement due to non-elastic deformations in the ballast and in the underlying soil can become so high that full contact between some sleepers and the ballast bed is lost. “Hanging” sleepers may then appear, inducing an irregularity of the track stiffness. Such situations may occur in embankment-to-bridge or tunnel transitions, when passing from ballasted to slab tracks and in regions where the railways cross underground structures. A numerical study on how to optimally select the track stiffness variation in the transition zone is presented in [1]. The objective function in the optimization procedure is related to the variation of the wheel/rail contact force. Soil improvement solutions, aiming to achieve a gradually variable stiffness profile between the different regions, are suggested. Another numerical study presented in [2] also evaluates the interaction force and the possibility of contact loss between the wheel and the rail.

Insight into the problem of induced vibrations can be acquired from simplified models, which have a closed form solution. Such approach has the following advantages: (i) only main results are available, so they are simple to analyse; (ii) the results preserve parameters dependence, allowing for direct sensitivity analysis; (iii) numerical evaluation can be carried out only in places of interest. Due to the simplifying assumptions, however, it must be stressed that the results obtained correspond only to an estimate of the structural response to a moving load.

There exist a large number of papers that are dealing with analytical solutions of problems involving vibrations of structures under moving loads. The methods implemented for obtaining the results depend mainly on the fact if the structure considered is finite or infinite. Of the wide range of problems involved, the problem of determining dynamic stresses in the beam structure, is the one which was solved first. Solutions were presented by Krylov [3] and later by Timoshenko [4]. Transversal vibrations in a simply supported beam traversed by a constant force moving at a constant velocity were presented by Inglis [5], Lowan [6] and later on other solutions have been presented by Koloušek [7] and Frýba [8]. In these approaches the results are usually expressed as an infinite sum of normal modes. Each mode contribution can be obtained by methods of integral transformation.

Transversal vibrations in an infinite beam on elastic foundation traversed by a constant force moving at a constant velocity were first evaluated by Timoshenko [9]. In this case, the beam is in a so-called quasi-stationary state, that is, at rest relative to the moving coordinate system. A moving coordinate system can thus be implemented and the solution can be expressed in a closed form with no sum required. Fourier integral transformation is used for solving the ordinary differential equation with respect to the moving coordinate variable. The more general case of a load variable in time is presented in [10].

When concerning non-homogeneous supports or foundation stiffness, it is relevant to mention a review on transition radiation in mechanics in [11]. The transition radiation in an infinite string resting on a non-homogeneous elastic foundation, represented by Winkler's model, is studied in [12]. The paper aims to compare the radiation due to an abrupt and a smooth change of parameters of the elastic foundation, when a constant load moves uniformly along the string. The problem is solved in the frequency as well as in the time domain. The analysis is restricted to subcritical velocities. In [13], transition radiations in other elastic systems are analysed. The work developed includes time domain response of an infinite Euler–Bernoulli beam on a non-homogeneous Winkler foundation subjected to a uniformly moving load. Further development is presented in [14], where, instead of the Winkler foundation, elastic half-planes are considered. The analytical solution presented in [13,14] has limits on the load travelling velocity, does not include the effect of damping, the evaluation procedure is numerically sensitive and, in fact, the method is suited for dealing with a single discontinuity traversed by a constant force. The solution in the region before the discontinuity is expressed as the known quasi-stationary part of that region and the unknown transient response in both regions. The transient parts satisfy the homogeneous governing equations of the problem. After the solution has been obtained, it can be used as an initial condition for obtaining the response in the region after the discontinuity. In this way, the radiation coming from the discontinuity only can be handled. In the supercritical range, however, there is radiation associated with the load motion itself, which makes this procedure more complicate. Nevertheless, the method has several advantages: the results are expressed in a closed analytical form, no sum is required and the solution is valid for a truly infinite structure. Further analytical study [15] adds a moving mass to the model and assumes periodicity of the inhomogeneous characteristics of the foundation stiffness. The main purpose is to determine conditions under which the vibrations become unstable.

In this paper, the dynamic response of a one-dimensional piece-wise homogeneous structure subjected to a time dependent transverse load moving at a constant velocity is expressed in an analytical form exploiting the normal-mode analysis. Discontinuities in the foundation stiffness parameter, in the flexural rigidity of the beam, in the mass per unit length or in the damping coefficient can be introduced. There is no restriction for finite structures, however, for infinite structures validity of the results is restricted to a “region of interest” (defined below) of finite length. Regarding the finite structures, “zones” are defined as the longest possible parts of the structure where all properties are homogeneous. It is assumed that the full structure is composed by a finite number of zones. The concept of the global dynamic stiffness matrix of the structure, which is a simple and reliable approach for dealing with the dynamic behaviour of beam systems with continuously distributed mass, is used to determine the natural frequencies and normal modes. This ensures that the natural frequencies are accurate. Although this method accurately deals with the dynamic behaviour of a distributed-parameter beam, it is not widely used. The reason is the numerical difficulty in evaluation of higher frequencies.

When a problem involving an infinite structure is under consideration, it is necessary to remove the effect of the supports: mitigate the perturbation by the boundary conditions themselves and prevent reflection of travelling waves. For

this purpose, in [16] implementation of semi-infinite parts at the extremities of the structure is suggested in a way which does not seem to be straightforward for implementation. In this paper, an alternative approach is presented and verified. Firstly, a “region of interest”, i.e., a part of the full structure where the results are supposed to be analysed, has to be defined. If the region of interest has finite length, it can be separated into a finite number of zones and the method proposed herein is suitable. The initial zone will be enlarged, the moving load will actuate further from the zone extremity and the load value will smoothly increase from zero to its full value along a “transition” region. A procedure for estimation of the length of such transition region is presented and the results obtained are verified. This does not bring additional computational cost, because all expressions are analytical and can be evaluated only within the region of interest. Also, the methodology presented is neither restricted by velocity magnitude nor by material or mass damping coefficients.

In summary, the main contributions of this paper consist of: (i) implementation of normal-mode analysis; (ii) formulation and results validation of a technique allowing to get results within a certain region (region of interest), as if they were obtained from an infinite beam; (iii) establishment of rules for numerical evaluation of the results. The procedures are programmed in MAPLE [17]. As an illustrative example of the methodology, the probability of an admissible upward displacement to be exceeded when a load passes with a certain velocity according to the normal distribution is determined. It is assumed that in the given structure, composed of two zones with different Winkler constants, there is an intermediate third zone of fixed length and adaptable foundation stiffness. The stiffness of that intermediate zone is optimized with respect to the maximum upward displacement in a parametric way.

With respect to the paper organization, Sections 2 and 3 deal with finite beams only. In Section 2, governing equations and simplifying assumptions are stated (for simplicity, only Euler–Bernoulli formulation is presented). In Section 3, the closed form solution is given and the concept of the global dynamic stiffness matrix for finite beams is explained. In Section 4, rules for the numerical expression of the results are established and a technique enabling results within a region of interest, as if they were obtained on infinite beam, is described. Section 5 shows verification examples, Section 6 presents the optimization of the stiffness of the intermediate zone and Section 7 summarizes the research achievements and further challenges. It is worth noticing that this work has direct application on the knowledge of ground vibrations induced by high-speed trains, especially when a train moves from a region to another with significantly different foundation stiffness.

## 2. Problem statement

Let a uniform motion of a time variable vertical force along a horizontal finite beam on a linear visco-elastic foundation be assumed. The foundation is modelled as a set of distributed springs and dashpots. Simplifications for the analysis of vertical vibrations are outlined as follows:

- (i) linear elastic Euler–Bernoulli theory is assumed;
- (ii) the beam damping is proportional to the velocity of vibration; and
- (iii) load inertia is neglected.

Taking into account the assumptions stated above, the equation of the forced vibration  $w(x,t)$  reads as [8]

$$\frac{\partial^2}{\partial x^2} \left( EI(x) \frac{\partial^2 w(x,t)}{\partial x^2} \right) + \mu(x) \frac{\partial^2 w(x,t)}{\partial t^2} + c(x) \frac{\partial w(x,t)}{\partial t} + k(x)w(x,t) = \delta(x-vt)P(t), \tag{1}$$

where  $EI$  represents the flexural rigidity,  $\mu$  the mass per unit length,  $c$  the damping coefficient,  $k$  the Winkler constant,  $w$  the transversal displacement,  $P$  the travelling force (considered positive when acting downwards),  $v$  the constant velocity,  $x$  the spatial coordinate (with origin at the left extremity of the structure),  $t$  the time and  $\delta$  the Dirac function. Zero time corresponds to the force position at  $x=0$ . Parameters  $EI$ ,  $\mu$ ,  $c$  and  $k$  can have piece-wise constant distribution along the structure. It is assumed that the full finite structure can be divided into a finite number of zones, where the beam and the foundation properties are homogeneous. An example of structure under consideration is shown in Fig. 1. In this representation, the structure is considered as simply supported and composed by two zones. Boundary conditions in this example read as

$$w(0,t) = 0, \quad w(L,t) = 0, \quad \left. \frac{\partial^2 w(x,t)}{\partial x^2} \right|_{x=0} = 0, \quad \left. \frac{\partial^2 w(x,t)}{\partial x^2} \right|_{x=L} = 0, \tag{2}$$

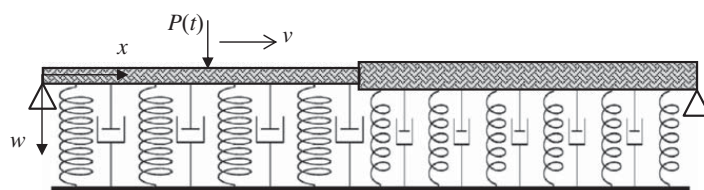


Fig. 1. Example of structure under consideration—finite simply supported beam composed of two zones.

where  $L$  is the total length of the structure. Initial conditions are assumed as homogeneous:

$$w(x, 0) = 0, \quad \left. \frac{\partial w(x, t)}{\partial t} \right|_{t=0} = 0. \tag{3}$$

It is allowed for time variation of the travelling force, although its velocity is maintained constant. No restriction is imposed on the velocity magnitude, as long as the normal-mode (mode superposition) method remains valid.

### 3. Problem solution

For finite beams, Eq. (1) can be solved by normal-mode analysis [7,8]:

$$w(x, t) = \sum_{j=1}^{\infty} q_j(t) w_j(x), \tag{4}$$

where  $q_j(t)$  are the generalized displacements and  $w_j(x)$  are the orthogonal natural modes normalized by

$$N_j = \sqrt{\int_0^L \mu(x) w_j^2(x) dx}, \tag{5}$$

where  $L$  it is the total length of the structure.

In order to calculate the undamped natural frequencies and the corresponding normal modes, the structure is divided into zones with homogeneous properties, i.e. constant values of  $EI$ ,  $\mu$ ,  $k$  or  $c$ . The damping coefficient  $c$  is obviously unnecessary for undamped vibrations; however, it will be seen later on Eqs. (13) and (15) that this coefficient must also be considered for zones identification. Contrary to what occurs in a finite element formulation, only as many zones as the given number of different properties are required, because the normal modes can be determined exactly in an analytical form within each zone.

Let the full structure be separated into  $n$  zones. The local dynamic stiffness matrix of  $s$ -th zone can be calculated in the following way. Its degrees of freedom are shown in Fig. 2a. Excitation with unit amplitude and given circular frequency  $\omega$  is assumed in direction of one of the degrees of freedom while the other degrees of freedom are kept fixed. For such excitation, member-end generalized harmonic forces in the steady-state regime (shown in Fig. 2b) are calculated. The procedure is repeated for the other degrees of freedom. The dynamic stiffness matrix is a symmetric  $4 \times 4$  matrix composed by harmonic functions with amplitudes shown as follows:

$$\begin{Bmatrix} V_{ik}^s \\ M_{ik}^s \\ V_{ki}^s \\ M_{ki}^s \end{Bmatrix} = \begin{bmatrix} \frac{EI_s}{L_s^3} F_6(\lambda_s) & -\frac{EI_s}{L_s^2} F_4(\lambda_s) & \frac{EI_s}{L_s^3} F_5(\lambda_s) & \frac{EI_s}{L_s^2} F_3(\lambda_s) \\ & \frac{EI_s}{L_s} F_2(\lambda_s) & -\frac{EI_s}{L_s^2} F_3(\lambda_s) & \frac{EI_s}{L_s} F_1(\lambda_s) \\ & & \frac{EI_s}{L_s^3} F_6(\lambda_s) & \frac{EI_s}{L_s^2} F_4(\lambda_s) \\ \text{symm.} & & & \frac{EI_s}{L_s} F_2(\lambda_s) \end{bmatrix} \cdot \begin{Bmatrix} \Delta_i^s \\ \varphi_i^s \\ \Delta_k^s \\ \varphi_k^s \end{Bmatrix}. \tag{6}$$

The terms in Eq. (6) make use of the following Kolousek's functions [7]:

$$\begin{aligned} F_1(\lambda_s) &= -\lambda_s \frac{\sinh \lambda_s - \sin \lambda_s}{\cosh \lambda_s \cos \lambda_s - 1}, & F_2(\lambda_s) &= -\lambda_s \frac{\cosh \lambda_s \sin \lambda_s - \sinh \lambda_s \cos \lambda_s}{\cosh \lambda_s \cos \lambda_s - 1}, \\ F_3(\lambda_s) &= -\lambda_s^2 \frac{\cosh \lambda_s - \cos \lambda_s}{\cosh \lambda_s \cos \lambda_s - 1}, & F_4(\lambda_s) &= \lambda_s^2 \frac{\sinh \lambda_s \sin \lambda_s}{\cosh \lambda_s \cos \lambda_s - 1}, \\ F_5(\lambda_s) &= \lambda_s^3 \frac{\sinh \lambda_s + \sin \lambda_s}{\cosh \lambda_s \cos \lambda_s - 1}, & F_6(\lambda_s) &= -\lambda_s^3 \frac{\cosh \lambda_s \sin \lambda_s + \sinh \lambda_s \cos \lambda_s}{\cosh \lambda_s \cos \lambda_s - 1}. \end{aligned} \tag{7}$$

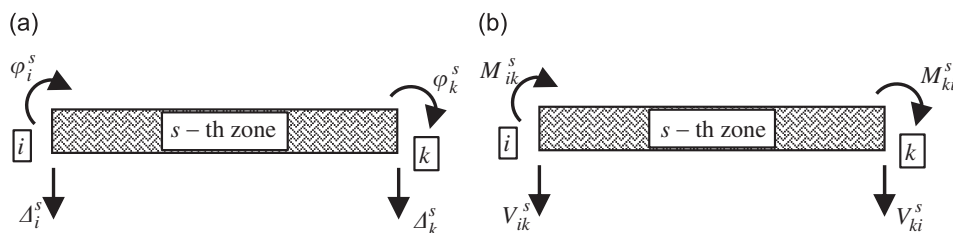


Fig. 2. (a) Degrees of freedom and (b) member-end generalized harmonic forces of the  $s$ -th zone with nodes  $i$  and  $k$ .

Parameters  $\lambda_s$  ( $s=1,2,\dots,n$ ), of the different zones are linked together with the excitation frequency as

$$\omega = \sqrt{\frac{\lambda_1^4 EI_1}{L_1^4 \mu_1} + \frac{k_1}{\mu_1}} = \sqrt{\frac{\lambda_2^4 EI_2}{L_2^4 \mu_2} + \frac{k_2}{\mu_2}} = \dots = \sqrt{\frac{\lambda_n^4 EI_n}{L_n^4 \mu_n} + \frac{k_n}{\mu_n}} \quad (8)$$

The global dynamic stiffness matrix is assembled by the direct stiffness method and its determinant is set to zero. The roots of this equation,  $\omega_j$ , are the natural frequencies. Substituting  $\omega = \omega_j$  back into the global matrix, unknown nodal displacements and rotations can be evaluated.

Normal modes are functions composed by well-defined parts within each zone and linked together by the nodal displacements and rotations. The natural undamped  $j$ -th mode of vibration in the  $s$ -th zone reads as

$$w_{sj}(x) = A_{sj} \sin \frac{\lambda_{sj}(x-L_{0s})}{L_s} + B_{sj} \cos \frac{\lambda_{sj}(x-L_{0s})}{L_s} + C_{sj} \sinh \frac{\lambda_{sj}(x-L_{0s})}{L_s} + D_{sj} \cosh \frac{\lambda_{sj}(x-L_{0s})}{L_s}, \quad s = 1, 2, \dots, n, \quad (9)$$

where

$$L_{0s} = \sum_{r=1}^{s-1} L_r$$

and  $L_r$  is the length of the  $r$ -th zone. Constants from Eq. (9) can be expressed as a function of the nodal displacements ( $A_i^s, A_k^s$ ) and rotations ( $\varphi_i^s, \varphi_k^s$ ):

$$\begin{aligned} C_{sj} &= \frac{1}{2\lambda_{sj}^3} F_6(\lambda_{sj}) A_i^s + \left( -\frac{L_s}{2\lambda_{sj}^3} F_4(\lambda_{sj}) + \frac{L_s}{2\lambda_{sj}} \right) \varphi_i^s + \frac{1}{2\lambda_{sj}^3} F_5(\lambda_{sj}) A_k^s + \frac{L_s}{2\lambda_{sj}^3} F_3(\lambda_{sj}) \varphi_k^s, \\ D_{sj} &= \left( \frac{1}{2\lambda_{sj}^2} F_4(\lambda_{sj}) + \frac{1}{2} \right) A_i^s - \frac{L_s}{2\lambda_{sj}^2} F_2(\lambda_{sj}) \varphi_i^s + \frac{1}{2\lambda_{sj}^2} F_3(\lambda_{sj}) A_k^s - \frac{L_s}{2\lambda_{sj}^2} F_1(\lambda_{sj}) \varphi_k^s, \\ A_{sj} &= \frac{L_s}{\lambda_{sj}} \varphi_i^s - C_{sj}, \\ B_{sj} &= A_i^s - D_{sj}. \end{aligned} \quad (10)$$

In order to determine the generalized coordinates of displacement,  $q_j(t)$ , it is necessary to transfer the governing equation into the time domain. According to the normal-mode analysis general steps, the loading function  $p(x, t) = \delta(x-vt)P(t)$  is expanded in series:

$$p(x, t) = \sum_{j=1}^{\infty} \mu(x) Q_j(t) w_j(x) \quad (11)$$

and  $Q_j(t)$  is calculated by multiplying Eq. (11) by  $w_k(x)$ , integrating over the whole structure and exploiting the orthonormality of the mode shapes with respect to the norm (5), as

$$Q_j(t) = \int_0^L p(x, t) w_j(x) dx, \quad (12)$$

where the subscript  $k$  was switched back to  $j$ . With  $Q_j(t)$  thus obtained, Eqs. (4) and (11) can be substituted into the governing equation (1). If the resulting equation is valid for all normal modes, the equation for  $q_j(t)$ , i.e. the equation of motion in principal coordinates, is deduced and solved by Laplace transformation. It yields for homogeneous initial conditions:

$$q_j(t) = \frac{1}{b_j(x)} \int_0^t Q_j(\tau) e^{-c(x)/2\mu(x)(t-\tau)} \sin(b_j(x)(t-\tau)) d\tau, \quad (13)$$

where

$$b_j(x) = \sqrt{\omega_j^2 - \left( \frac{c(x)}{2\mu(x)} \right)^2}, \quad (14)$$

which for a concentrated force (point load), simplifies as

$$q_j(t) = \frac{1}{b_j(x)} \int_0^t P(\tau) w_j(v\tau) e^{-c(x)/2\mu(x)(t-\tau)} \sin(b_j(x)(t-\tau)) d\tau. \quad (15)$$

Extension of this method to more complex structural conditions considering effect of shear distortion, rotational inertia, axial force, intermediate visco-elastic layers, etc., is straightforward. The only issue is to establish the local dynamic stiffness matrix of the zones. Some of these matrices are already available in [7,16,18].



#### 4. Numerical implementation

##### 4.1. Natural frequencies, mode shapes and time integration

Although the expressions presented in the previous section are rather simple, difficulties arise regarding the numerical expression of the results. In particular, determination of natural frequencies is considered the most complex part of the numerical assessment. This difficulty is aggravated by the fact that a very high number of natural frequencies is usually required in problems with foundation stiffness or other parameters discontinuities. An author's previous work [19] focused on avoiding the natural frequencies evaluation and suggested a different procedure. The deflection field was calculated by linking together, using continuity conditions, the analytical solutions of each structural zone.

In the present work, several possibilities of obtaining natural frequencies were examined:

- (i) commercial finite element software;
- (ii) built-in procedures in commercial numerical and symbolic computation software;
- (iii) own procedure programmed in programming language; and
- (iv) own procedure programmed in commercial numerical and symbolic computation software.

Regarding (i), the commercial general purpose finite element software ANSYS [20] was tested. According to [21], the error in higher natural frequencies is inherent to the standard finite element method. Hence, many elements must be used for obtaining higher frequencies with acceptable accuracy. However, it was observed that the error in the frequencies of the flexural modes obtained with ANSYS exceeded significantly the error established analytically in [21]. This can be explained by the intrinsic numerical error associated to the eigenvalues extraction procedure.

A simply supported beam was chosen to assess the numerical error. In this case, the natural frequencies can be expressed analytically by

$$\omega_j = \sqrt{\left(\frac{j\pi}{L}\right)^4 \frac{EI}{\mu} + \frac{k}{\mu}} \quad (16)$$

Two standard European rails UIC60 with a length of 100 m were chosen to represent the beam. The corresponding flexural rigidity and mass per unit length are summarized in Table 1. Block Lanczos extraction method and consistent mass matrix, and preconditioned conjugate gradient (PCG) Lanczos extraction method and lumped mass matrix were used to determine the first 500 natural frequencies. The results are summarized in Fig. 3. It is seen that the error can reach 29 percent in the 500-th mode. In fact, the analytical value of that frequency is very high (12 848 Hz), out of the range considered in high-speed train applications, but the graphs indicate that the error tends to increase substantially for high frequencies. ANSYS numerical value is lower than the analytical one, while the opposite tendency is predicted analytically in [21]. On the other hand, the fundamental frequency obtained by the PCG Lanczos extraction method and lumped mass matrix is higher than the analytical value, but the error in fundamental frequency for 5000 elements is –17 percent. This error is hardly visible in the graph of Fig. 3d because the second frequency error is much less (in absolute value). Next, the effect of an elastic foundation was tested. It was found that the error in the natural frequencies error is basically independent on the value of the foundation stiffness when Block Lanczos extraction method and consistent mass matrix are used. Two different models of the ANSYS library, element BEAM54 with the capacity of introduction of elastic foundation and element BEAM3 with added discrete springs at each node, gave the same results.

After that, other parameters were varied and it was observed that the error (for a given beam length) is higher for higher ratios of the flexural rigidity to the mass per unit length of the beam. When the beam was considered as the full track (representative values are  $EI=66.7 \text{ MN m}^2$  and  $\mu = 7200 \text{ kg/m}$ , leading to a higher  $EI/\mu$  ratio), the error in the 500-th frequency reached 78.5 percent. The corresponding analytical value is 3779 Hz, much lower than in the previous case. Another aggravating factor was detected when Block Lanczos extraction method and consistent mass matrix were used.

**Table 1**  
Numerical input data used in examples.

Property	Beam (2 rails UIC60)
Young's modulus $E$ (GPa)	210
Moment of inertia $I$ ( $\text{m}^4$ )	$6110 \times 10^{-8}$
Mass per unit length $\mu$ ( $\text{kg m}^{-1}$ )	119.87
	Foundation
Winkler constant per unit length in soft region—verification study: $k_1$ ( $\text{kN m}^{-2}$ )	427
Winkler constant per unit length in strong region—verification study: $k_2$ ( $\text{kN m}^{-2}$ )	854
Winkler constant per unit length in soft region—parametric study ( $\text{kN m}^{-2}$ )	1000
Winkler constant per unit length in strong region—parametric study ( $\text{kN m}^{-2}$ )	10 000
	Load
Maximum force applied $P_0$ (kN)	166.8

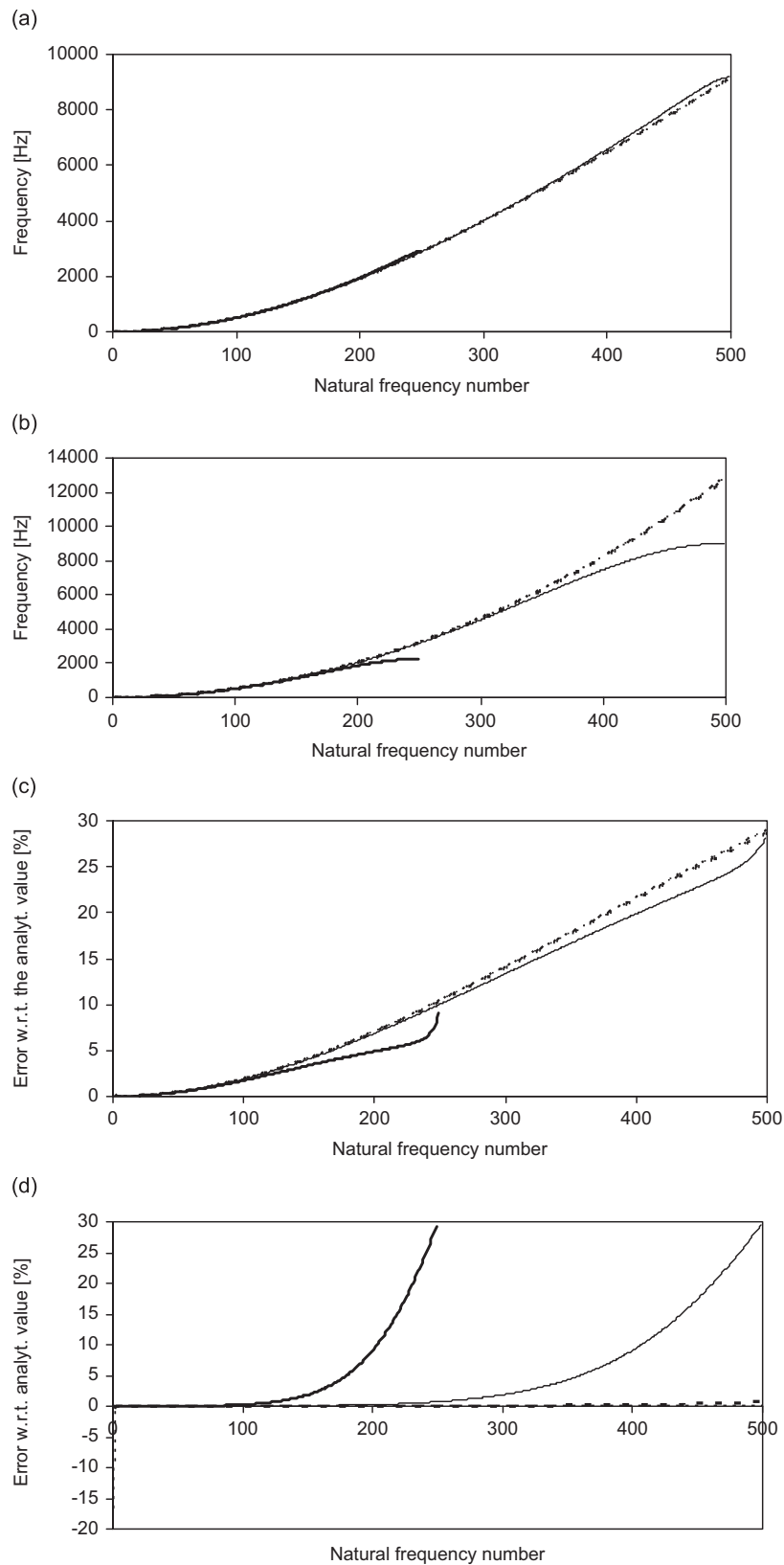


**Fig. 3.** Numerical values and the error in natural frequencies of simply supported beam (250 elements—full bold line, 500 elements—full line, 1000 elements—dotted bold line, 5000 elements—dotted line): (a) numerical value: block-Lanczos extraction method and consistent mass matrix, (b) numerical value: preconditioned conjugate gradient Lanczos extraction method and lumped mass matrix, (c) error: block-Lanczos extraction method and consistent mass matrix, (d) error: preconditioned conjugate gradient Lanczos extraction method and lumped mass matrix.



The values of the first natural frequencies are numerically proximate, which can disorder their sequence. For instance, for a foundation stiffness of  $10 \text{ MN m}^{-2}$ , the first three modes are interchanged in a way that the expected first mode-shape appears in the third position. For a foundation stiffness of  $40 \text{ MN m}^{-2}$ , the same situation occurs for the first seven modes (see Fig. 4), and for  $100 \text{ MN m}^{-2}$  the first 11 mode shapes are interchanged among themselves. For the previous case of 2UIC60 rails, when a foundation stiffness of  $100 \text{ MN m}^{-2}$  is adopted, the first five mode shapes are interchanged. In these cases, the total length  $L=100 \text{ m}$  was discretized into 5000 finite elements. More complicated cases were not tested because it was concluded that commercial finite element software is not suitable to provide the natural frequencies values and mode shapes for further usage in Eq. (4) and later. Therefore attention will be switched to the possibility of using the global dynamic stiffness matrix for natural frequencies and normal modes determination.

For examination of the other options (ii–iv), the global dynamic stiffness matrix has to be prepared first. Let the full structure is composed of  $n$  zones. After the global matrix has been assembled, Eq. (8) can be substituted and the determinant can be expressed in terms of a single unknown,  $\omega$ . Actually, it is more convenient to express the determinant in terms of  $\omega^2$  and search for  $\omega^2$  instead of  $\omega$ . Except for very simple cases, the determinant contains a quite complicated combination of trigonometric and hyperbolic functions, requiring numerical search of the roots. The determinant has many singularities coincident with all natural frequencies of each zone considered separately. This is because the denominator consists of a product of expressions:  $H_s(\lambda_s)$ ,  $s=1, \dots, n$ . For  $s=2, \dots, n-1$ ,  $H_s(\lambda_s) = \cosh \lambda_s \cos \lambda_s - 1$ , which correspond to the left hand side of the characteristic equation of each “internal” zone (all but the initial and the final). The expressions for the first and final zones,  $H_1(\lambda_1)$  and  $H_n(\lambda_n)$ , can be different, depending on the actual boundary conditions at the extremities of the structure. To better deal with the singularities, it is suggested in [18] to use smaller zones. However, the approach proposed, in contrary, has the advantage of allowing implementation of zones as large as possible. In order to avoid special treatment around the singularities, it is possible to solve the roots only in the numerator. As mentioned above, the roots in the denominator correspond to the natural frequencies of each zone considered separately, therefore they cannot coincide with the natural frequency of the full structure. Mathematically this statement can be supported by the fact, that the “existence” of the denominator is the consequence of the implementation of the member-end generalized forces, in order to simplify the assemblage of the global dynamic stiffness matrix. Expression coincident with the numerator would be possible to obtain by the determinant of the full matrix, composed by the coefficients of the constants  $A_s, B_s, C_s, D_s$ ,  $s=1, \dots, n$  from Eq. (9), if four conditions of continuity (for displacement, rotation, transverse force and bending moment) in each structural node were applied on the deflection expression given by Eq. (9).

For the numerical search of the roots, a software able to handle very large numbers and introduce high-digits precision must be used. Programming languages (FORTRAN, C++) and software for numerical calculation (MATLAB) were tested. Double precision immediately inhibited the usage of these programs. Very high numbers were impossible to attain, as well. For instance, the last possible integer argument of function “exp” in MATLAB is 709. It will be justified by convergence studies in Section 5 that such argument is not sufficient. In contrary, the symbolic calculation software MAPLE allowed to: (a) increase number of digits used in evaluation without any link to the computer specified value; (b) deal with very high numbers. Therefore, all procedures for numerical evaluation of the results were programmed in MAPLE environment.

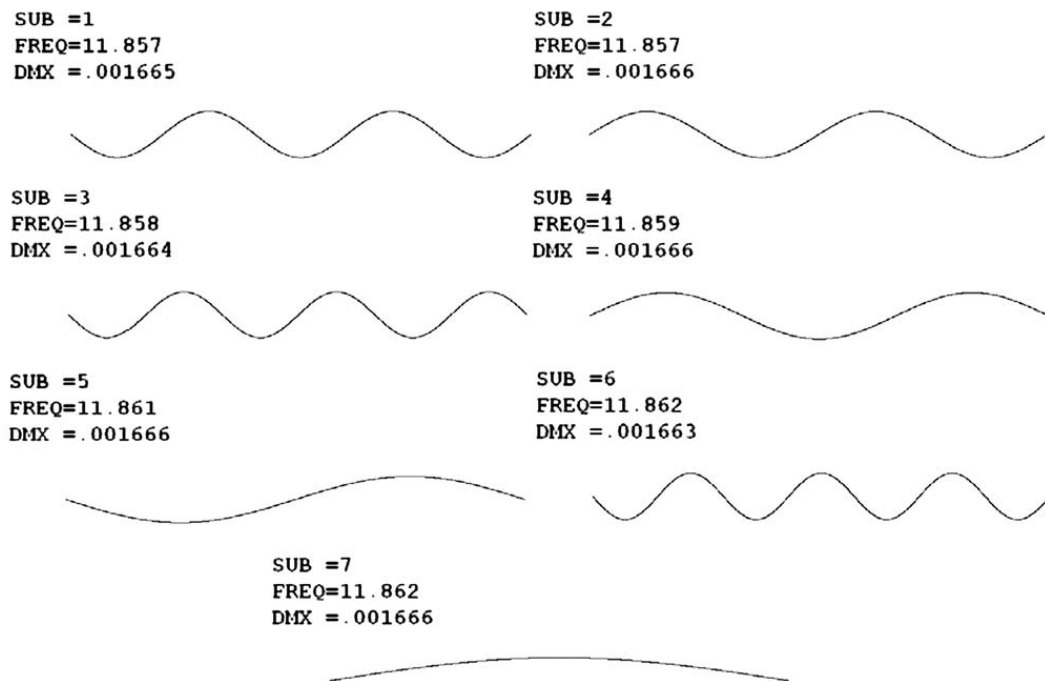


Fig. 4. Disorder in natural modes of simply supported beam on elastic foundation: results obtained in ANSYS.

Nevertheless, built-in MAPLE routines failed to find the roots. After several tries, an own procedure based on the bisection method was implemented. This procedure is fast when reasonable estimates are used. For the sake of simplicity, the process of getting such estimates is explained under the assumption that all discontinuities have origin in the elastic foundation parameter  $k$ . Due to the nature of the problem, roots are separated by  $\sqrt{k_s/\mu}$ , or in fact by  $k_s/\mu$  because  $\omega^2$  is sought for. Values  $k_s/\mu$  also yield zero determinant, but, as they correspond to the rigid motion of the structural zone, have no contribution to the final shape. Let  $k_s$  be ordered increasingly. Then, no roots occur below  $k_1/\mu$ . Roots within the interval  $(k_1/\mu; k_2/\mu)$  correspond to natural frequencies, for which the corresponding mode shape affects only the softest region. The first root in this interval can be thus estimated according to the expected mode shape. Moreover, roots progressively increase their distance in each interval  $(k_s/\mu_s; k_{s+1}/\mu_{s+1})$ ,  $s=1,2,\dots,n-1$ , and  $(k_n/\mu_n; \infty)$ . This allows estimation of the next root position. Implementation of these estimates can make the procedure for finding the roots very efficient. In several seconds, more than 1000 natural frequencies with  $10^{-32}$  precision can be found. The required precision of the roots can be easily adapted. Working precision should be around 40–60 digits, depending on the problem. Simple checking procedures can be implemented, in order to verify that no frequencies are missing.

In order to express numerically the mode shapes, Eq. (9) must be adapted. It was found that reliable results even in 16-digits precision can be achieved using the form presented below:

$$w_{sj}(x) = (\Delta_{i,sj}G_1(\lambda_{sj}, L_s, L_{0s}) + \varphi_{i,sj}G_2(\lambda_{sj}, L_s, L_{0s}) + \Delta_{k,sj}G_3(\lambda_{sj}, L_s, L_{0s}) + \varphi_{k,sj}G_4(\lambda_{sj}, L_s, L_{0s})) / (2\lambda_{sj}(\cosh \lambda_{sj} \cos \lambda_{sj} - 1)), \quad s = 1, 2, \dots, n, \quad (17)$$

where for instance

$$G_1(\lambda_{sj}, L_s, L_{0s}) = \lambda_{sj} \left\{ -\cos\left(\frac{\lambda_{sj}(x-L_{0s})}{L_s} - \lambda_{sj}\right) - \cosh\left(\frac{\lambda_{sj}(x-L_{0s})}{L_s} - \lambda_{sj}\right) + \cosh\left(\frac{\lambda_{sj}(x-L_{0s})}{L_s}\right) \cos(\lambda_{sj}) + \sinh\left(\frac{\lambda_{sj}(x-L_{0s})}{L_s}\right) \sin(\lambda_{sj}) + \cos\left(\frac{\lambda_{sj}(x-L_{0s})}{L_s}\right) \cosh(\lambda_{sj}) - \sin\left(\frac{\lambda_{sj}(x-L_{0s})}{L_s}\right) \sinh(\lambda_{sj}) \right\}. \quad (18)$$

Again, Eq. (17) should be used in MAPLE or similar symbolic calculation software, because a large argument (beyond 709) is common in the problems presented herein. Eq. (18) might look unnecessarily complicated, but it was verified as the most reliable way for performing both the numerical evaluation of the mode shapes and the analytical expression of the time integrals from Eq. (15). The time integration window is separated in few time intervals. Limits of these intervals (except for the current time  $t$ ) correspond only to instants at which the load reaches a structural node or has an alteration in its description (see Eq. (19), explained in the next section). Thus, numerical values of  $q_i(t)$  can be calculated very quickly only in times of interest.

#### 4.2. Extension to infinite beams

In this section, a technique which allows obtaining results within the region of interest as if were calculated on infinite beams is presented. If the region of interest has finite length, it can be divided into a finite number of zones and the method proposed here is suitable. The initial zone will be enlarged, the moving load will be let to actuate further from the zone extremity and the load value will be let to smoothly increase from zero to its full value along a transition region. Then, the length of the initial zone is separated into three lengths: initial  $L_i$ , transition  $L_c$  and remaining  $L_r$ , which already contain a part of the region of interest. This separation does not bring additional computational cost, because all expressions are analytical and therefore can be evaluated only within the region of interest. The extremities of the full structure can be supported or free, just resting on the elastic foundation, because these regions are out of the region of interest. It is assumed that the force starts to actuate at  $L_i$  and that it varies from zero to its final value over a transition region  $L_c$ . The time variation of the force is assumed to have a sinusoidal shape in order to keep the time derivatives continuous. In more detail

$$P(t) = \begin{cases} 0 & \text{for } t \leq \frac{L_i}{v}, \\ \frac{P_0}{2} \left( 1 + \sin\left(\pi \left(\frac{vt}{L_c} - \frac{L_i}{L_c} - \frac{1}{2}\right)\right) \right) & \text{for } \frac{L_i}{v} < t \leq \frac{L_i+L_c}{v}, \\ P_0 & \text{for } t > \frac{L_i+L_c}{v}, \end{cases} \quad (19)$$

where  $P_0$  is the final value of the force applied. This technique ensures that the maximum displacement smoothly increases until reaching its final value, which corresponds to the analytical maximum of the quasi-stationary regime. The question is how to determine  $L_i$  and  $L_c$ . For that purpose, analogy with a representative spring can be used. For the sake of simplicity, it is assumed that the force applied increases linearly. Thus, let a ramped force with a maximum value  $F$  be applied on a mass  $m$  supported by a spring of rigidity  $K$ . Time variation of the mass displacement can be expressed analytically by

$$u(t) = \frac{F}{K} + \frac{F\sqrt{m}}{t_c\sqrt{K^3}} \left( \sin\left(\sqrt{\frac{K}{m}}(t-t_c)\right) - \sin\left(\sqrt{\frac{K}{m}}t\right) \right), \quad (20)$$

where  $t_c$  is the time during which the force increases linearly. The second term on the right hand side of Eq. (15) stands for the oscillating part of the solution. The amplitude of this oscillation is:

$$\frac{F}{t_c} \sqrt{\frac{2m \left( 1 - \cos \left( \sqrt{\frac{K}{m}} t_c \right) \right)}{K^3}} \quad (21)$$

When considering a lower time  $t_c$ , the amplitude gets generally higher, but there is an additional oscillation of the amplitude itself. For our purpose, it is enough to choose the time  $t_c$  in a way to force the amplitude to a “reasonable” part of  $F/K$ . This requirement does not depend on the force applied, but only on  $m$  and  $K$ . In accordance with this analogy,  $K$  can be replaced by  $k$  and  $m$  by  $\mu$ . This technique will be validated in the next section.

It would be possible to assume in Eq. (20) only linear variation of the force applied. Nevertheless, it was verified numerically, by comparing results obtained for different values of  $L_i$  and  $L_c$  and sinusoidal versus linear load variation, that continuity of the time derivatives of the load variation function prevents possible oscillations of the final value. Oscillation in this context means that the maximum displacement obtained within the region of interest does not exactly match the analytical value of the quasi-stationary regime but shows slight variation in time with respect to its “target” value.

## 5. Verification examples

In the verification examples, the general methodology and the technique described in Section 4.2 are validated. Therefore, the objective of these examples is to compare the results obtained in the region of interest with previous work [13] and also, in order to validate the technique from Section 4.2, to test the results obtained in the region of interest for checking independency on the boundary conditions of the full structure.

Two UIC60 rails are used to model the beam. The load applied has a total axle mass of 17 000 kg corresponding to a locomotive of the Thalys high-speed train. All numerical input data are summarized in Table 1. Very weak foundation conditions are assumed, as in [13], in order to better visualize the deflection field and for the sake of comparison. Values of  $k_1=427 \text{ kN m}^{-2}$  and  $k_2=854 \text{ kN m}^{-2}$  are adopted for the soft and the strong regions, respectively. Two velocities,  $v=180$  and  $230 \text{ m s}^{-1}$ , are considered. Lengths of the two zones with different foundation stiffness are taken as 1000 m. The justification of this choice is given later on in this section. Boundary conditions are assumed in two ways, modelling a clamped–clamped and a free–free beam.

As the main objective of this paper is to analyse the effect of an abrupt change in the foundation stiffness, the structure response should be studied around this change. Hence, the limits of the region of interest are located 100 m before and after the discontinuity. According to the analogy presented in the previous section, it can be verified that, for the data specified and a velocity below  $230 \text{ m s}^{-1}$ ,  $L_c = 600 \text{ m}$  ensures that the maximum amplitude taken from Eq. (21) lies below 1.3 percent of the maximum value, which is acceptable.  $L_i = 100 \text{ m}$  and  $L_r = 300 \text{ m}$  (containing 100 m of the region of interest of the first zone) were chosen. Therefore, a total length of  $1000+1000 \text{ m}$  for the full structure is used. The first 1000 m region is separated as  $100+600+300 \text{ m}$  as explained above. Over the last length of 300 m, the force applied maintains its maximum value  $P_0$ . No changes are introduced in the second 1000 m region.

As mentioned above,  $k_1=427 \text{ kN m}^{-2}$  is introduced in the soft region and  $k_2=854 \text{ kN m}^{-2}$  in the strong one. Such weak foundation allows implementation of velocities close to the critical one, while still remaining in the range of realistic values. The closer to the critical velocity, the higher is the ratio between the upward and the downward maximum displacement of the quasi-stationary solution. Under these conditions, the increase in the displacement field with respect to the stationary shape is better visualized. According to [8], the critical velocities corresponding to steady-state situations with homogeneous foundation  $k=427$  and  $854 \text{ kN m}^{-2}$  are:  $197.6$  and  $235.0 \text{ m s}^{-1}$ , respectively. Therefore, the two tested velocities  $v=180$  and  $230 \text{ m s}^{-1}$  have the following meaning: the former one is subcritical in both regions and the latter one is subcritical in the strong and supercritical in the soft region. The latter velocity has a rather academic sense for it cannot yet be achieved by any train.

At first, the procedure outlined in Section 4.2 is validated. Three ways of validation were chosen:

- independency of the solution within the region of interest on the boundary conditions of the full structure. Clamped–clamped beam and free–free beam, as two fundamentally different situations of finite beam, were chosen in order to prove that the effect of boundary conditions within the region of interest is irrelevant;
- comparison of the solution obtained within the region of interest with [13]; and
- verification of the quasi-stationary deflection shape according to [8] within the region of interest in the first zone, before reaching the discontinuity.

The evolution of the displacement field was calculated over the full structure, although only the region of interest is used for validation. The case of  $v=180 \text{ m s}^{-1}$  and passage from the soft to the strong regions (passage forward) is presented. In Fig. 5a, displacement under force is plotted over the full length of the structure for the two different boundary conditions referred to above. It is seen that both curves match perfectly within the region of interest. After the initial and transition lengths  $L_i$  and  $L_c$  have been surpassed, the displacement achieves its analytical value of the stationary solution

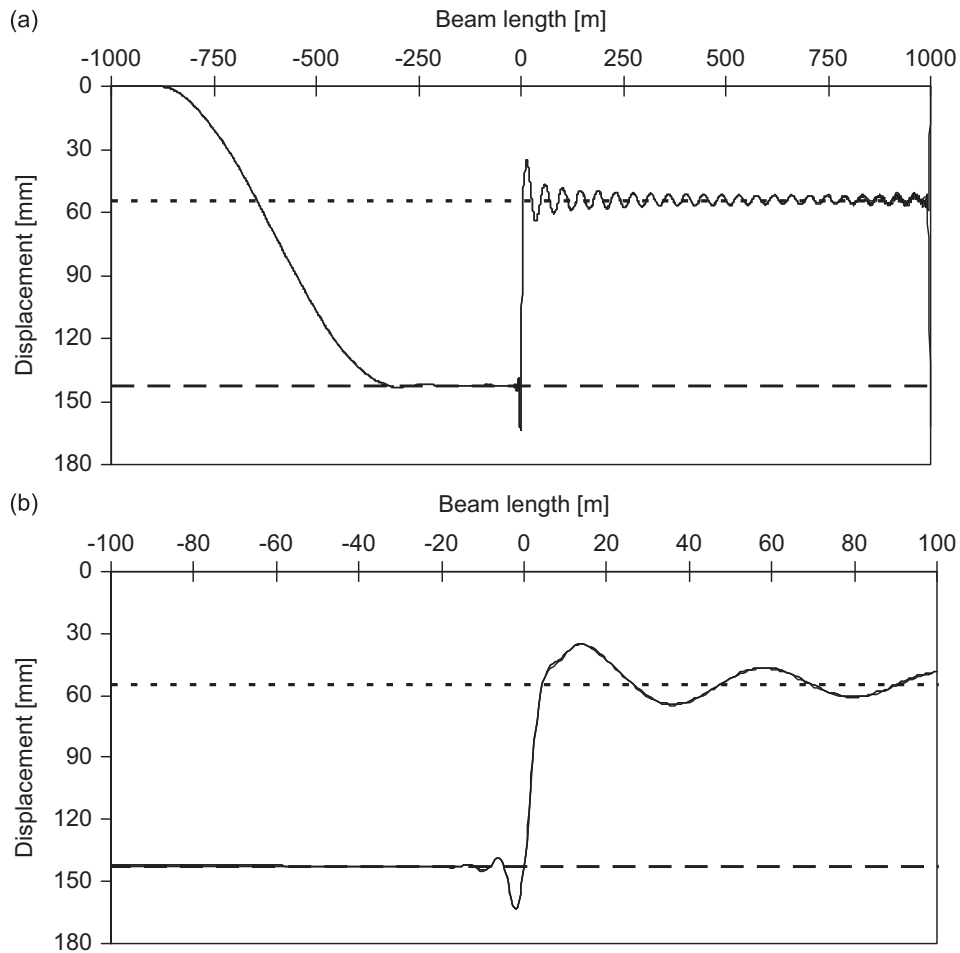


**Fig. 5.** Displacement under the force, passage forward with velocity  $v=180 \text{ m s}^{-1}$ : (a) full length, (b) region around the foundation discontinuity. Dashed lines are used for the quasi-stationary solutions.

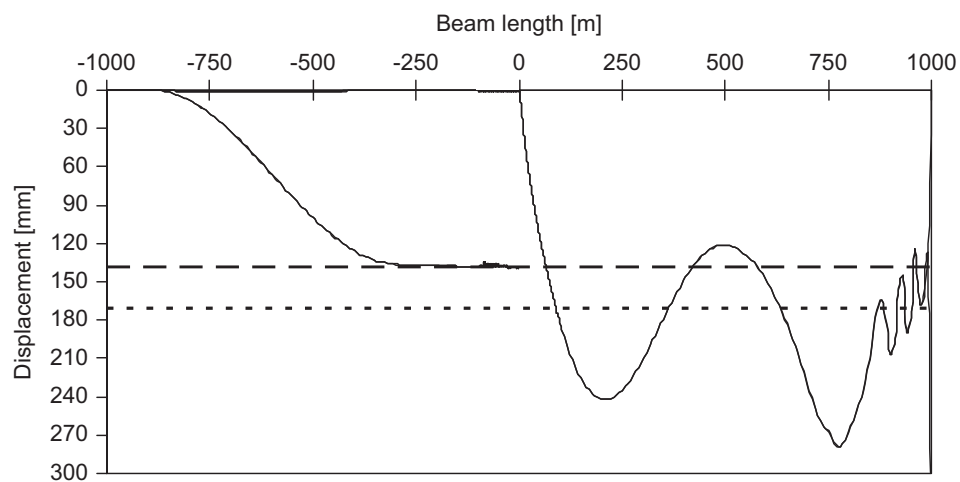


**Fig. 6.** Displacement under the force and maximum downward displacement in the first part of the structure, passage forward with velocity  $v=230 \text{ m s}^{-1}$ . Dashed lines are used for the quasi-stationary solutions.

for an infinite beam without noticeable oscillations. Then, there occurs disturbance due to the foundation discontinuity: the maximum displacement slightly oscillates and after it stabilizes at the analytical value of the second region. In Fig. 5b only the region of interest is shown. Comparison is done with the results presented in [13]. All curves obtained match exactly each other. The same situation is presented in Fig. 6 for the velocity  $v=230 \text{ m s}^{-1}$ . In this case, the method from [13] is not valid anymore, therefore it is not considered. The velocity is supercritical in the soft region, yielding zero displacement under the force in the first region. The maximum downward oriented displacement (behind the force) is also

plotted in Fig. 6, but only within the first region. This value can be compared with the analytical value of the quasi-stationary regime.

The deflection field in the beam within the region of interest is represented in Figs. 7–16. Vertical displacements are plotted at several load positions. Each figure contains the results for both boundary conditions. The displacement field is compared with the solution presented in [13]. For  $\nu=180 \text{ m s}^{-1}$ , when that solution is still valid, curves match perfectly; for  $\nu=230 \text{ m s}^{-1}$ , significant differences are verified. In the first load positions (Figs. 7 and 12), the displacement according to [18] for quasi-stationary state is added. Except for solution [13], for  $\nu=230 \text{ m s}^{-1}$  all curves are indistinguishable, thus there is no legend added in figures. In the subcritical case it is seen that the maximum downward displacement is reached

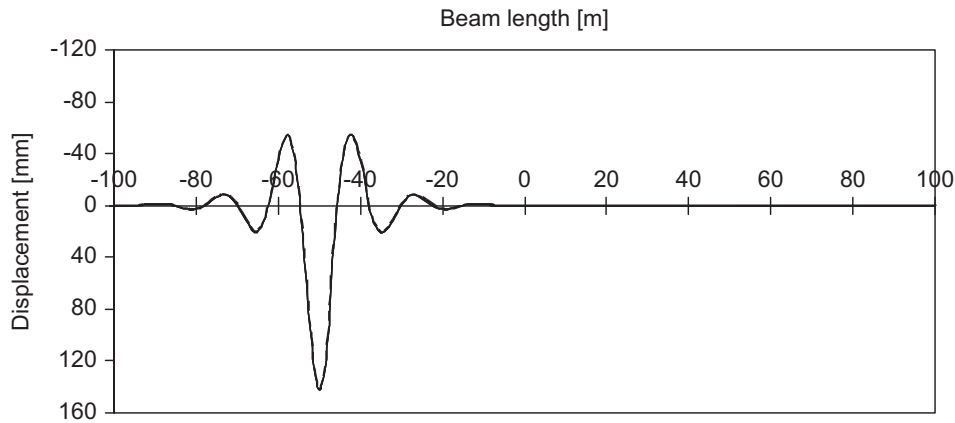


Fig. 7. Passage forward with velocity  $\nu=180 \text{ m s}^{-1}$ , four overlapped curves corresponding to both boundary conditions, solution from [13] and quasi-stationary state from [8], load position at  $-50 \text{ m}$ .

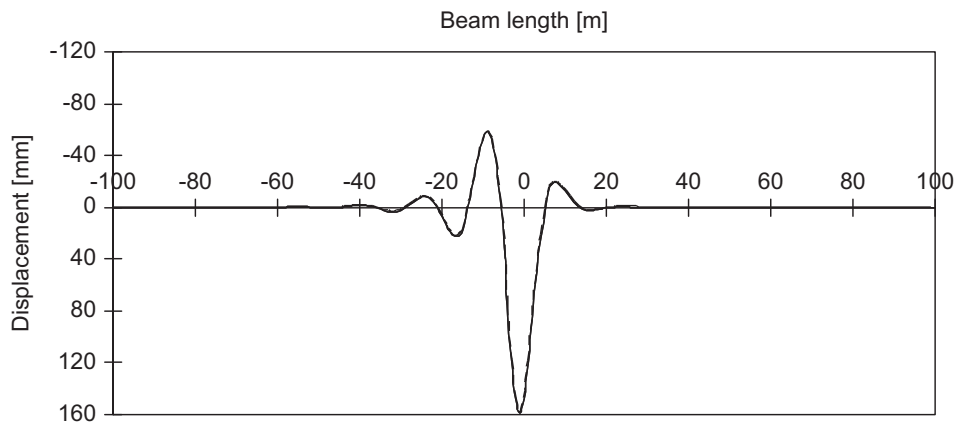


Fig. 8. Passage forward with velocity  $\nu=180 \text{ m s}^{-1}$ , three overlapped curves corresponding to both boundary conditions and solution from [13], load position at  $-1 \text{ m}$ .

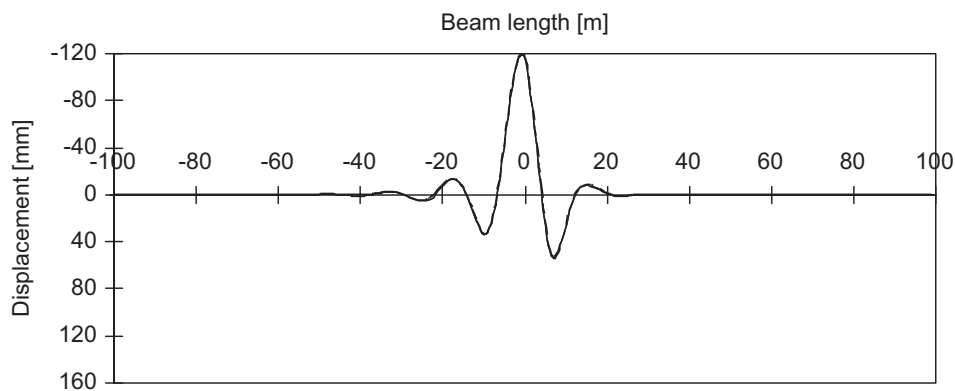
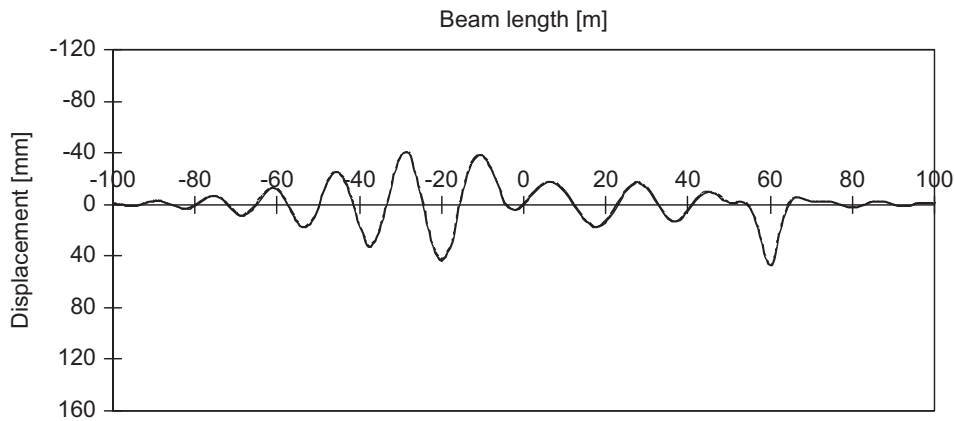
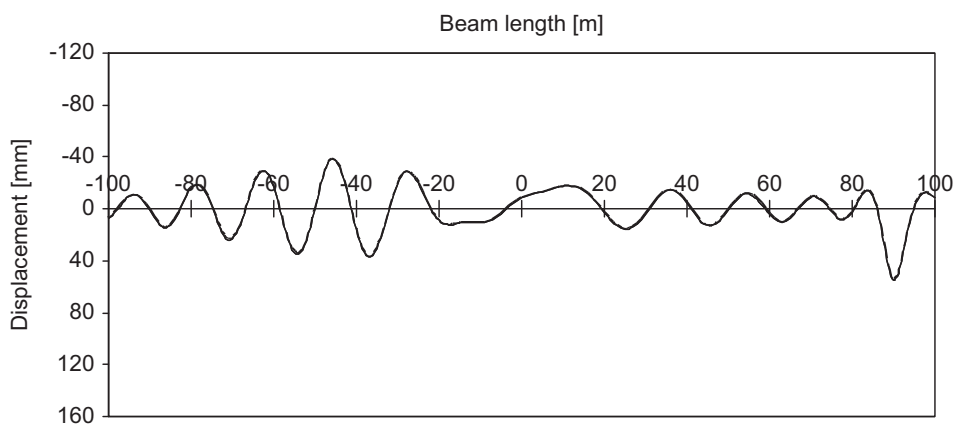


Fig. 9. Passage forward with velocity  $\nu=180 \text{ m s}^{-1}$ , three overlapped curves corresponding to both boundary conditions and solution from [13], load position at  $6 \text{ m}$ .



**Fig. 10.** Passage forward with velocity  $v=180\text{ m s}^{-1}$ , three overlapped curves corresponding to both boundary conditions and solution from [13], load position at 60 m.



**Fig. 11.** Passage forward with velocity  $v=180\text{ m s}^{-1}$ , three overlapped curves corresponding to both boundary conditions and solution from [13], load position at 90 m.

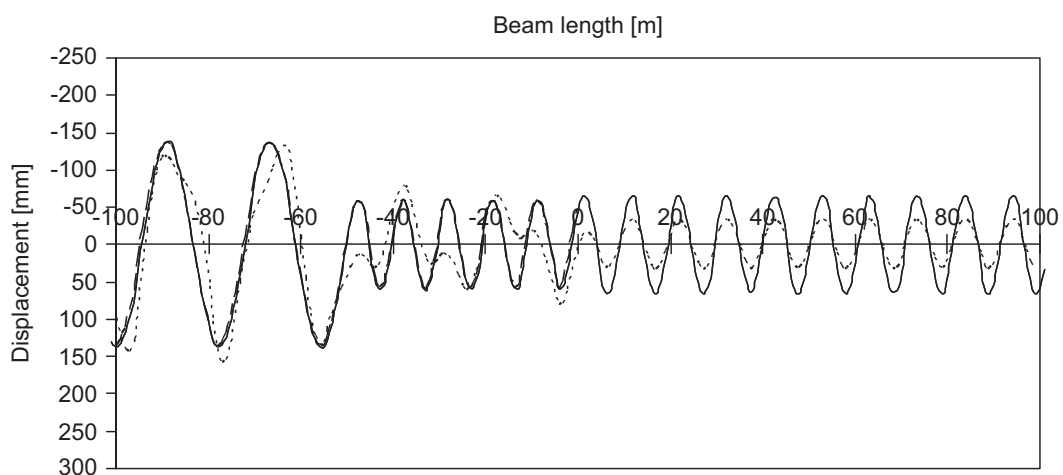


**Fig. 12.** Passage forward with velocity  $v=230\text{ m s}^{-1}$ , three overlapped curves corresponding to both boundary conditions and the quasi-stationary state from [8], solution from [13] is represented by the dashed curve, load position at  $-50\text{ m}$ .

right before the discontinuity (Fig. 8) and the maximum upward one at basically the same location, but short time after the force has traversed the discontinuity (Fig. 9).

Thousand natural modes were used, corresponding to the last implemented frequency of 129 Hz. Such large number of modes is justified by convergence studies, presented in Fig. 17. Two curves for each velocity are plotted. They correspond to two characteristic displacements. Regarding the velocity  $180\text{ m s}^{-1}$ , position at 1 m before the discontinuity, when the force is acting at the same position (Fig. 8) and at 6 m after the discontinuity (Fig. 9) was chosen. For velocity  $230\text{ m s}^{-1}$ ,

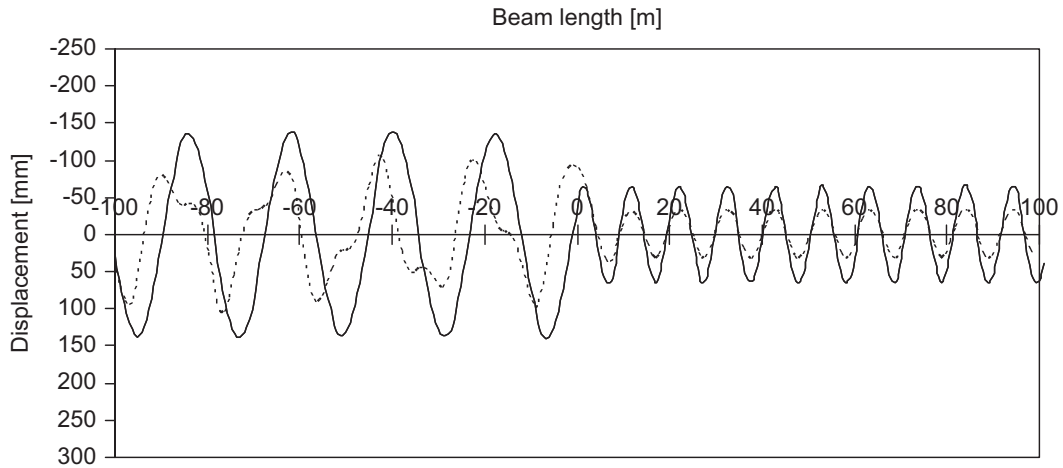


**Fig. 13.** Passage forward with velocity  $v=230\text{ m s}^{-1}$ , two overlapped curves corresponding to both boundary conditions, solution from [13] is represented by the dashed curve, load position at  $-1\text{ m}$ .

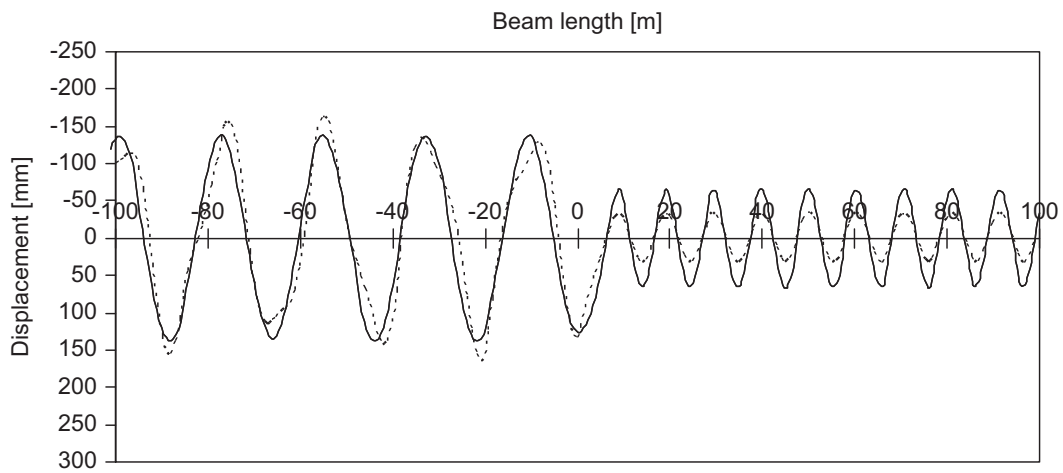


**Fig. 14.** Passage forward with velocity  $v=230\text{ m s}^{-1}$ , two overlapped curves corresponding to both boundary conditions, solution from [13] is represented by the dashed curve, load position at  $6\text{ m}$ .

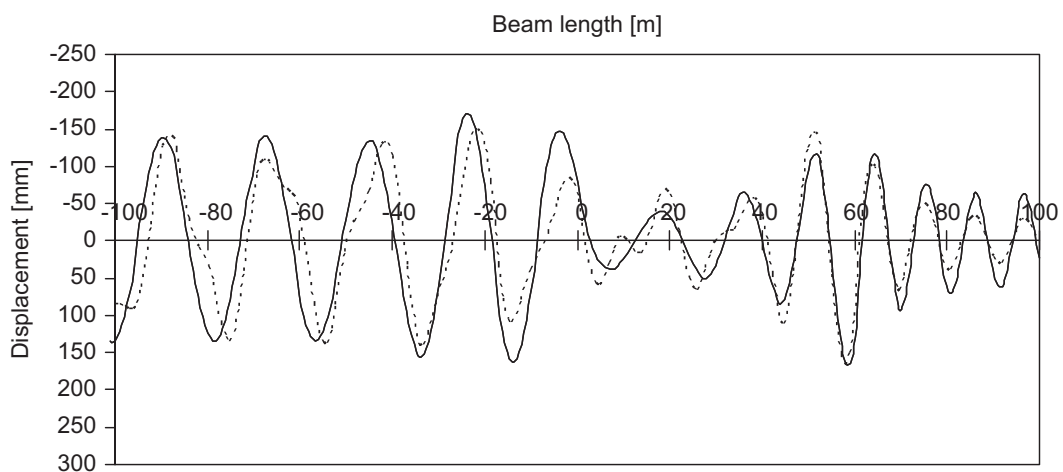


**Fig. 15.** Passage forward with velocity  $v=230\text{ m s}^{-1}$ , two overlapped curves corresponding to both boundary conditions, solution from [13] is represented by the dashed curve, load position at  $60\text{ m}$ .

force acting at  $90\text{ m}$  after the discontinuity (Fig. 16) and positions  $4\text{ m}$  before and  $89\text{ m}$  after the discontinuity were selected. It is seen that around  $700$  modes would be sufficient, but since the increase to  $1000$  modes does not imply much larger computational cost,  $1000$  were used in order to guarantee high accuracy of the results. It is necessary to point out



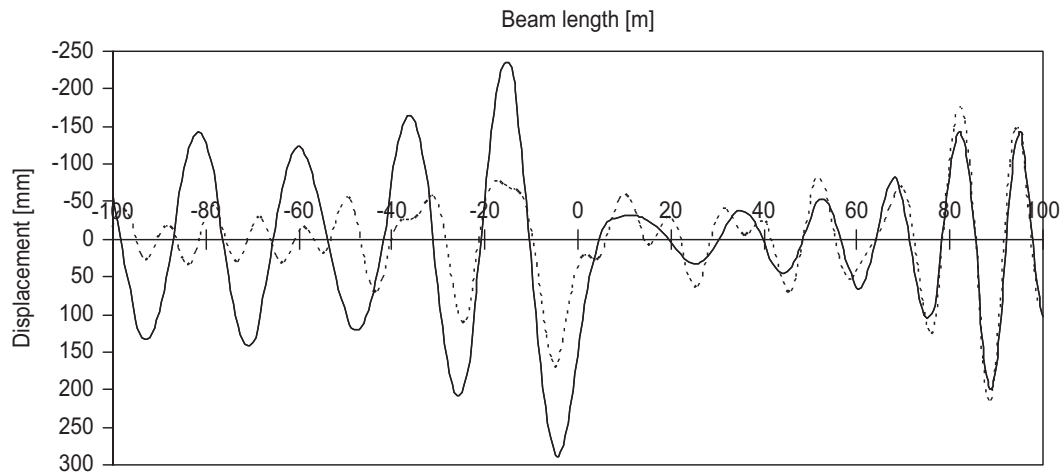


**Fig. 16.** Passage forward with velocity  $v=230 \text{ m s}^{-1}$ , two overlapped curves corresponding to both boundary conditions, solution from [13] is represented by the dashed curve, load position at 90 m.

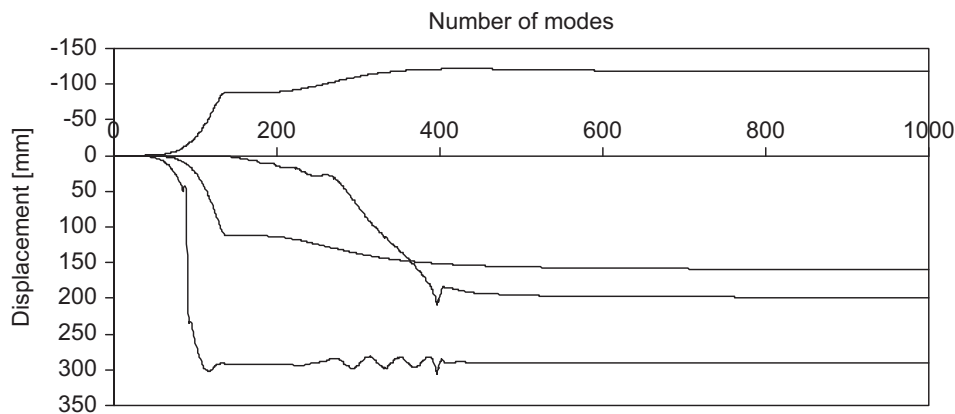


**Fig. 17.** Convergence study—curves from top to bottom: velocity  $180 \text{ m s}^{-1}$ , position at 1 m before, load position at 6 m after the discontinuity; velocity  $180 \text{ m s}^{-1}$ , position at 1 m before, load position at 1 m before the discontinuity; velocity  $230 \text{ m s}^{-1}$ , position at 89 m after, load position at 90 m after the discontinuity; and velocity  $230 \text{ m s}^{-1}$ , position at 4 m before, load position at 90 m after the discontinuity.

that in the verification example the first 136 modes affect only the soft part of the structure, which already indicates that a large number of modes will be necessary in the analysis. Reminding the question of large arguments, it is worthwhile to point out that the argument 709 is exceeded already in the 444-th mode in the soft region. Such number of modes is certainly not sufficient, as obvious from Fig. 17.

A good isolation device and ideal rail surface was assumed in the previous analysis, therefore the harmonic component was neglected and the load was modelled as a constant moving force. Nevertheless, the harmonic component of the load could also be easily implemented in the methodology.

## 6. Parametric optimization of intermediate region

To illustrate the utility of the methodology, the probability of exceeding an admissible upward displacement when the load crosses at a certain velocity according to the normal distribution, is determined. For this optimization problem, it is assumed that the given structure has an intermediate zone of adaptable foundation stiffness. The length of this intermediate zone is fixed and its foundation stiffness is optimized. In the study shown below, Winkler constant in the soft region is taken as  $1000 \text{ kN m}^{-2}$ , in the strong one is 10 times higher, i.e.  $10\,000 \text{ kN m}^{-2}$ , and the intermediate zone length is chosen as 6 m, covering therefore 10 sleepers. Lengths of the soft and of the strong zones, their separation, number of implemented modes and other numerical data are the same as in the previous study. Reference velocity is chosen as  $150 \text{ m s}^{-1}$ , obeying normal distribution with standard deviation of  $3 \text{ m s}^{-1}$ . Passage of the load in both directions is investigated.

The analysis is performed in a parametric way with respect to the velocity and the intermediate foundation stiffness. During the analysis, the velocity is varied by  $10 \text{ m s}^{-1}$  steps from  $140$  to  $160 \text{ m s}^{-1}$ , to accommodate the chosen standard deviation. The maximum upward displacement was selected as the most harmful effect in this analysis. Evolution of this displacement with the load position is shown in Fig. 18 for a structure without an intermediate zone. Regarding the

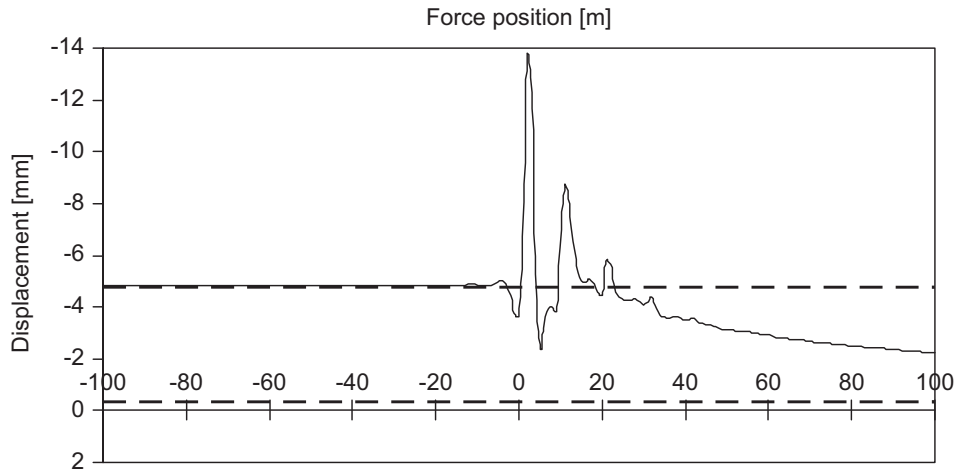


Fig. 18. Maximum upward displacement, passage forward with velocity  $\nu=150\text{ m s}^{-1}$ , dashed lines are used for the quasi-stationary solutions.

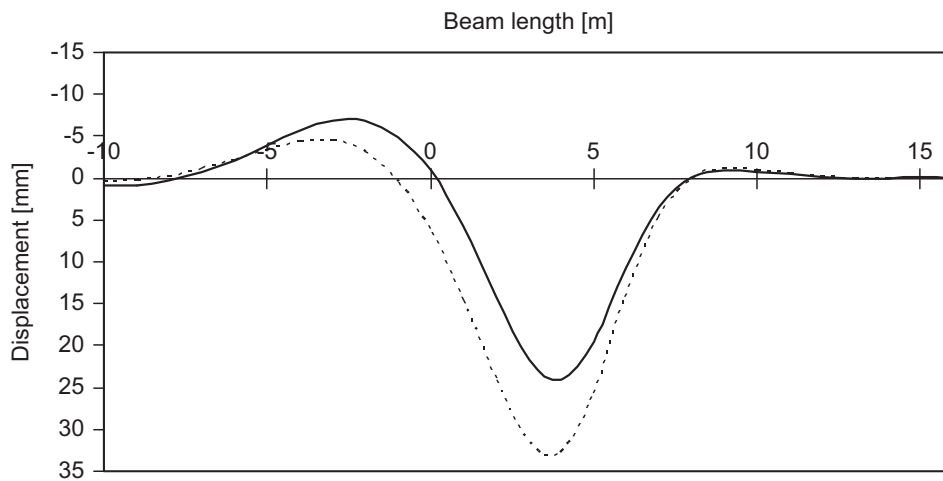
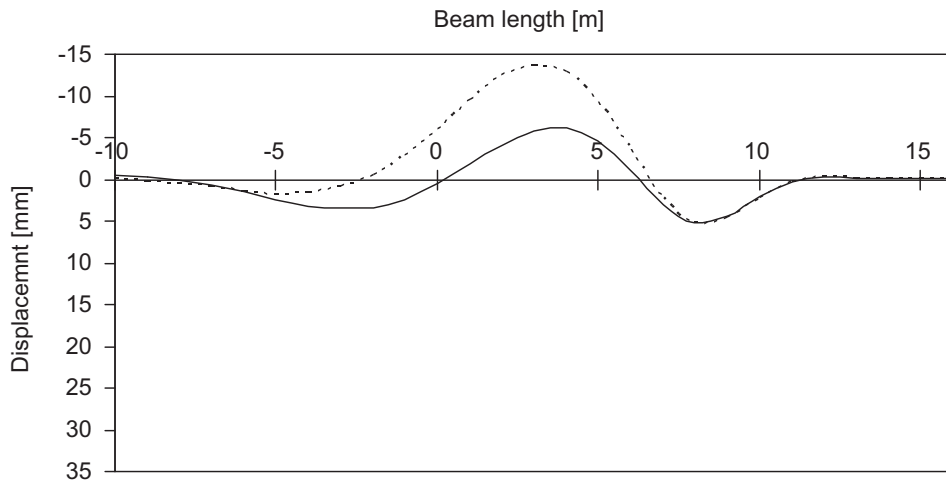


Fig. 19. Displacement from the optimized solution (full curve) compared with the solution without the intermediate region (dotted curve), load position at 4 m when the maximum in the optimized solution is achieved.

passage forward, the results of optimization show that a very small increase in foundation stiffness with respect to the soft value will attenuate the displacement peak in the soft region and, at the same time, will ensure that the displacement shape is affected in a way that the next discontinuity in foundation stiffness does not cause a large peak in the response (Figs. 19 and 20). A 50 percent reduction on the displacements was obtained by the optimization procedure. Similar features were observed for the opposite load movement (passage backward), although only a reduction of 28 percent was achieved. Figs. 21 and 22 show the maximum displacement as a function of the velocity for the forward and the backward passage. It is seen that a stiffness of  $1400\text{ kN m}^{-2}$  is the optimum value for the passage forward while  $1500\text{ kN m}^{-2}$  corresponds to the optimum for the passage backward. The displacement values are compared in Table 2. In Figs. 23 and 24 the deflection curves around the intermediate zone are presented. Each curve corresponds to a different velocity. The curves selected are the ones where the maximum upward displacement was attained. The deflection shape indicates the load position in such cases. For the passage forward, the maximum is always achieved at the same load position. However, this is not verified for the passage backward. Results are affected by the step chosen for the numerical evaluation (1 m). The main advantage of this analysis is the fact that an analytical solution is used, therefore in each case only a small region before and after the intermediate region needs to be analysed to find the maximum. A 10 m-length is enough for the passage forward, while slightly more is necessary for the passage backward (a 20 m-length was used). Thus, the regions of interest were taken as 26 and 46 m for the passage forward and backward, respectively.

An important conclusion of this analysis is the fact that the optimum intermediate stiffness for the forward and the backward passage are very similar, which is quite significant for practical use. In order to complete the optimization analysis, admissible values of 7 and 8 mm for the upward displacement were chosen. The probability of exceeding them is summarized in Table 3. It can be concluded that the optimum intermediate stiffness for this problem is  $1400\text{ kN m}^{-2}$  and the probability of exceeding admissible displacements of 7 and 8 mm is 70.7 and 30.4 percent, respectively.



**Fig. 20.** Displacement from the optimized solution (full curve) compared with the solution without the intermediate region (dotted curve), load position at 8 m when the maximum in the non-optimized solution is achieved.

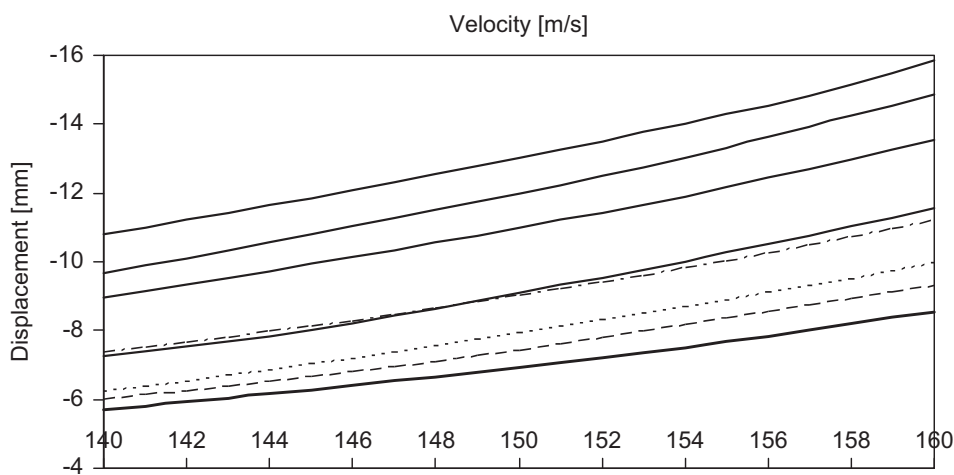


**Fig. 21.** Maximum upward displacement as a function of velocity, passage forward. Bold curve shows the optimum solution ( $1400 \text{ kN m}^{-2}$ ), the closest values are for  $1500 \text{ kN m}^{-2}$  (dashed),  $1600 \text{ kN m}^{-2}$  (dotted),  $1200 \text{ kN m}^{-2}$  (dot-and-dash line), other four full curves refer to 2000, 3000, 4000,  $8000 \text{ kN m}^{-2}$  (the highest).

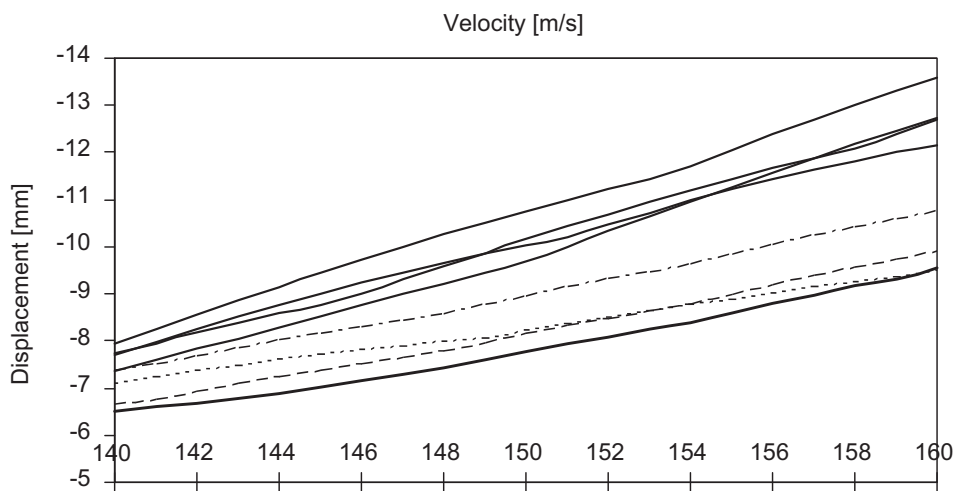


**Fig. 22.** Maximum upward displacement as a function of velocity, passage backward. Bold curve shows the optimum solution ( $1500 \text{ kN m}^{-2}$ ), the closest values are for  $1400 \text{ kN m}^{-2}$  (dashed),  $1600 \text{ kN m}^{-2}$  (dotted),  $1200 \text{ kN m}^{-2}$  (dot-and-dash line), other four full curves refer to 2000, 3000, 4000,  $8000 \text{ kN m}^{-2}$  (the highest).

**Table 2**

Maximum upward displacement for the passage by the reference velocity.

Maximum upward displacement (mm)	Passage forward ( $v=150 \text{ m s}^{-1}$ )	Passage backward ( $v=150 \text{ m s}^{-1}$ )
No intermediate part	13.72	10.83
Intermediate stiffness $1400 \text{ kN m}^{-2}$	6.92	8.13
Intermediate stiffness $1500 \text{ kN m}^{-2}$	7.42	7.77

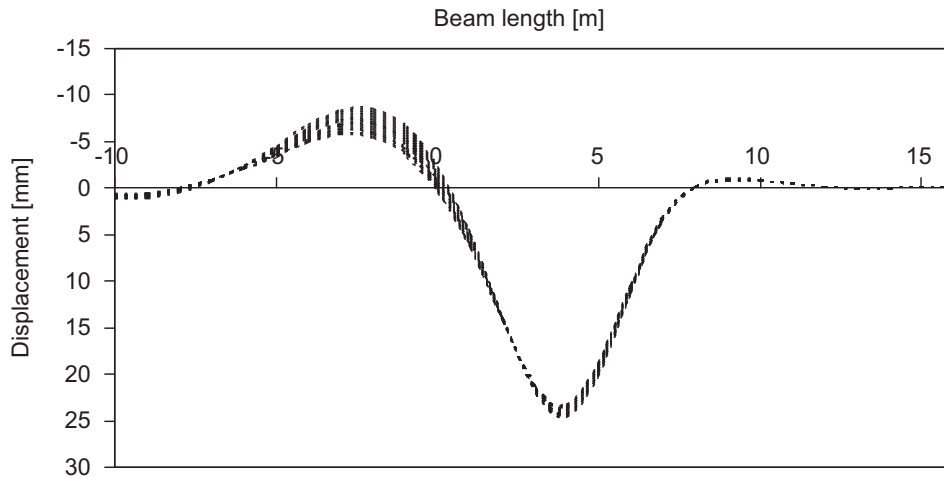


**Fig. 23.** Maximum upward displacement curves, passage forward. Zero position is at the first discontinuity. Each curve corresponds to a different velocity.

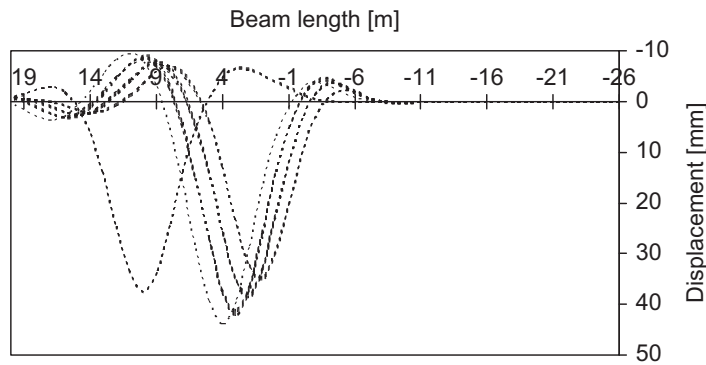


**Fig. 24.** Maximum upward displacement curves, passage backward. Zero position is at the first discontinuity. Each curve corresponds to a different velocity.

**Table 3**

Probabilities of exceeding the admissible values.

Probability	Admissible value 8 mm			Admissible value 7 mm		
	Passage forward (%)	Passage backward (%)	Total (%)	Passage forward (%)	Passage backward (%)	Total (%)
Intermediate stiffness $1400 \text{ kN m}^{-2}$	1.0	59.7	30.4	42.2	99.3	70.7
Intermediate stiffness $1500 \text{ kN m}^{-2}$	14.0	31.9	23.0	79.9	95.7	87.8

## 7. Conclusions and further development

The transversal vibrations induced by a load moving uniformly along a finite and an infinite beam resting on a piecewise homogeneous visco-elastic foundation have been investigated. Special attention has been paid to the amplification of these vibrations, originated by the load passage over a foundation discontinuity. The governing equations of the problem have been solved by normal-mode analysis. Procedures were programmed in MAPLE environment. The displacement field

was presented in a closed form as an analytical result, therefore if the problem under consideration does not concern full time history, numerical evaluation can be focused on selected places of interest, which significantly speeds up the analysis. Results presented show high level of accuracy, because they do not contain the error of the standard finite element method and the calculated natural frequencies and shapes are accurate.

The methodology presented has restrictions neither on load velocity magnitude nor on damping implementation. Loading can be represented by a set of moving forces which magnitudes can be time dependent. The beam can contain finite number of discontinuities in properties parameters. The main contribution lies in: (i) implementation of the normal-mode analysis; (ii) formulation and results validation of a technique allowing to get results within a certain region (region of interest), as if they were obtained on an infinite beam; and (iii) definition of rules for numerical evaluation of the results.

To illustrate the utility of the methodology, the probability of exceeding an admissible upward displacement of 7 and 8 mm when the load crosses at the velocity  $150 \text{ m s}^{-1}$  obeying the normal distribution, was determined. It was concluded that the optimized intermediate stiffness is basically the same for the passage forward and backward and that it corresponds to a small increase of the soft value. For the passage forward, the improvement is more significant than for the passage backward.

The methodology has some additional potentialities that can be explored in the future work. Among them it might be mentioned: (i) effect of several travelling forces; (ii) implementation of more complicated structural zones like an elevated railway, which can be modelled as a layered-beam system composed of two parallel beams with a visco-elastic layer in between, etc.; (iii) effect of the mass of the load; and (iv) extension to Timoshenko's beam.

Although focusing only on one-dimensional systems under physical and geometrical linearity, this study provides an important insight into the problem of excessive ground vibrations induced by high-speed trains passing in sections where an abrupt change in vertical stiffness occurs. It is worthwhile to mention that a detailed finite element analysis of the track and subgrade structure provides a very large amount of results which are not easy to handle and analyse. In fact, very refined meshes must be used in regions of stiffness discontinuities and the problem must be solved over the whole time domain, which is time consuming. Furthermore, in standard finite element codes higher natural frequencies are not accurately evaluated [21]. This error cannot be solved by refining the mesh, because it is inherent to the standard finite element formulation that makes use of cubic Hermite shape functions for the beam elements. The so-called "optical branches" of the discrete spectra diverge with polynomial degree, which shows that higher-order finite elements do not yield good approximation for higher modes in vibration analysis. Moreover, this error is usually aggravated by the numerical error of the eigenvalues extraction procedure itself. Having this in mind, the results presented herein are obtained faster and in a more accurate way than the ones obtained by means of standard finite element codes.

The results obtained have direct application on the analysis of railway track vibrations induced by high-speed trains when crossing regions with significantly different foundation stiffness. The conclusions of this paper might serve as a basis for the design of solutions for such regions.

## References

- [1] A. Lundqvist, T. Dahlberg, Railway track stiffness variations—consequences and countermeasures, *Proceedings of the 19th IAVSD Symposium on Dynamics of Vehicles on Roads and on Tracks*, Milan, Italy, 29 August–2 September, 2005.
- [2] A.C. Ribeiro, R. Calçada, R. Delgado, Track-train dynamic behaviour on transition zones of high speed railway lines, *Proceedings of the 11th International Conference on Civil, Structural and Environmental Engineering Computing*, St. Julians, Malta, 18–21 September 2007.
- [3] A.N. Krylov, Über die erzwungenen Schwingungen von gleichförmigen elastischen Stäben, *Mathematische Annalen* 61 (1905) 211–234 (in German).
- [4] S.P. Timoshenko, Forced vibration of prismatic bars, *Izvestiya Kievskogo politekhnicheskogo instituta* (in Russian), 1908;; S.P. Timoshenko, Erzwungene Schwingungen prismatischer Stäbe, *Zeitschrift für Mathematik und Physik* 59 (2) (1911) 163–203 (in German).
- [5] C.E. Inglis, *A Mathematical Treatise on Vibration in Railway Bridges*, The Cambridge University Press, Cambridge, 1934.
- [6] A.N. Lowan, On transverse oscillations of beams under the action of moving variable loads, *Philosophical Magazine, Series 7* 19 (127) (1935) 708–715.
- [7] V. Koloúšek, Dynamics of civil engineering structures—part I: general problems, second ed.—part II: continuous beams and frame systems, second ed.—part III: selected topics, SNTL, Prague, 1967, 1956, 1961, *Dynamics in Engineering Structures*, Academia, Prague, Butterworth, London, 1973 (in Czech).
- [8] L. Frýba, *Vibration of Solids and Structures under Moving Loads*, third ed., Research Institute of Transport, Prague (1972), Thomas Telford, London, 1999.
- [9] S.P. Timoshenko, Statical and dynamical stresses in rails, *Proceedings of the 2nd International Congress for Applied Mechanics*, Zürich (Switzerland), 12–17 September 1926, pp. 407–418.
- [10] L. Frýba, Infinite beam on an elastic foundation subjected to a moving load, *Aplikace Matematiky* 2 (2) (1957) 105–132 (in Czech).
- [11] A.I. Vesnitskii, A.V. Metrikine, Transition radiation in mechanics, *Physics—Uspekhi* 39 (1996) 983–1007.
- [12] A.V. Metrikine, A.R.M. Wolfert, H.A. Dieterman, Transition radiation in an elastically supported string. Abrupt and smooth variations of the support stiffness, *Wave Motion* 27 (1998) 291–305.
- [13] K.N. Van Dalen, Ground Vibration Induced by a High-speed Train Running over Inhomogeneous Subsoil, Transition Radiation in Two-dimensional Inhomogeneous Elastic Systems, Master Thesis, Department of Structural Engineering, TUDelft, 2006.
- [14] K.N. van Dalen, A.V. Metrikine, Transition radiation of elastic waves at the interface of two elastic half-planes, *Journal of Sound and Vibration* 310 (2008) 702–717.
- [15] S.N. Verichev, A.V. Metrikine, Instability of vibrations of a mass that moves uniformly along a beam on a periodically inhomogeneous foundation, *Journal of Sound and Vibration* 260 (2003) 901–925.
- [16] Y.-H. Chen, Z.-M. Shiu, Resonant curves of an elevated railway to harmonic moving loads, *International Journal of Structural Stability and Dynamics* 4 (2004) 237–257.
- [17] Release 11.0 Documentation for MAPLE, Maplesoft, a division of Waterloo Maple Inc., 2007.
- [18] Y.-H. Chen, J.-T. Sheu, Beam length and dynamic stiffness, *Computer Methods in Applied Mechanics and Engineering* 129 (1996) 311–318.
- [19] Z. Dimitrovová, J.N. Varandas, Critical velocity of a load moving on a beam with a sudden change of foundation stiffness: applications to high-speed trains, *Computers & Structures* 87 (2009) 1224–1232.
- [20] Release 11.0 Documentation for ANSYS, Swanson Analysis Systems IP, Inc., 2007.
- [21] J.A. Cottrell, A. Reali, Y. Bazilevs, T.J.R. Hughes, Isogeometric analysis of structural vibrations, *Computer Methods in Applied Mechanics and Engineering* 195 (2006) 5257–5296.